



Cite this: *New J. Chem.*, 2021, **45**, 5013

# Hydrogenolysis of glycerol in an aqueous medium over Pt/WO<sub>3</sub>/zirconium phosphate catalysts studied by <sup>1</sup>H NMR spectroscopy†

Susmita Bhowmik,  Nagasuresh Enjamuri and Srinivas Darbha \*

Bifunctional Pt/WO<sub>3</sub>/zirconium phosphate catalyzes the liquid-phase hydrogenolysis of glycerol in an aqueous medium. <sup>1</sup>H NMR spectroscopy (solvent suppression pulse program) is employed to monitor this reaction. Propanediols (1,3 + 1,2-PDO) formed as the major product along with propanols (1- and 2-POs) as the minor product. A synergistic enhancement in glycerol conversion and selectivity to 1,3-PDO was observed when both Pt and WO<sub>3</sub> were present in the catalyst. A *volcano-shape* variation of catalytic activity with W content was observed. A catalyst with 8 wt% W and 1 wt% Pt exhibited the highest selective hydrogenolysis performance (glycerol conversion = 92.3% and total PDOs selectivity = 45.9% and 1,3-PDO selectivity = 20.8% at 200 °C). Dispersed Pt in contact with polytungstate-type WO<sub>3</sub> species was found to be the active catalytic site. <sup>1</sup>H NMR spectroscopy is demonstrated as an attractive technique to *quantify* the products of a glycerol hydrogenolysis reaction.

Received 13th November 2020,  
Accepted 10th February 2021

DOI: 10.1039/d0nj05557c

[rsc.li/njc](http://rsc.li/njc)

## 1 Introduction

Hydrogenolysis of glycerol, a by-product of the modern oleochemical industry, to propanediols (1,2- and 1,3-PDOs) is of great importance, as these diols are the building-block chemicals of polymers, paints, cleaning products, carpets, adhesives and personal care items.<sup>1,2</sup> Considerable progress in catalyst development for 1,2-PDO has already been achieved.<sup>3,4</sup> But the conversion of glycerol to 1,3-PDO is more challenging. The 2°-OH group of glycerol is sterically hindered by the two 1°-OH groups, making it less accessible to the active sites in the catalyst. The activation energies for dehydration of 1°- and 2°-OH groups (based on neutral glycerol) are similar (70.9 kcal mol<sup>-1</sup> for 2°-OH and 73.2 kcal mol<sup>-1</sup> for 1°-OH) and the proton affinities are also nearly the same (195.4 kcal mol<sup>-1</sup> for 2°-OH and 194.8 kcal mol<sup>-1</sup> for the 1°-OH group).<sup>5</sup> These small differences in reactivity make it difficult to achieve high selectivity to 1,3-PDO. A moderate temperature operation is needed as high temperature leads to deep hydrogenolysis. Water is contained in raw bio-glycerol and it is also formed as a co-product in the glycerol hydrogenolysis reaction. Thus, it makes more sense to develop a catalytic process for glycerol in an aqueous medium to avoid the expensive distillation step for

forming ultra-pure glycerol reactant from bio-glycerol. Catalysts with strong acidity are the best choice for 1,3-PDO formation. But most of the acid catalysts are sensitive to aqueous medium and result in poor yield of 1,3-PDO.<sup>6</sup> All these limitations demand efficient catalysts for 1,3-PDO formation from aqueous glycerol. Among the reported solid catalysts,<sup>7</sup> supported Ir-ReO<sub>x</sub> and Pt-WO<sub>x</sub> are the most studied ones as they are more active and selective toward 1,3-PDO, due to adequate synergy between the metal oxide and metal nanoparticles. Tomishige and co-workers<sup>8-11</sup> found that ReO<sub>x</sub>-modified Ir supported on SiO<sub>2</sub> catalyzes this reaction under mild conditions (~120 °C, 80 bar, 12–24 h) and converts glycerol into 1,3-PDO with good activity by the direct dehydroxylation approach. In another study, Arundhathi *et al.*<sup>12</sup> disclosed a highly selective boehmite-based Pt/WO<sub>x</sub>/AlOOH catalyst which catalyzes the reaction at 180 °C and 50 bar H<sub>2</sub>. Several groups extended the studies and probed the influence of the support, metal loading and additives on the performance of a Pt-WO<sub>x</sub> catalyst.<sup>13-20</sup>

Zirconium phosphates (ZrP) are layered materials present in different forms depending on the method of preparation.<sup>21</sup> Their acidity, high thermal and chemical stability and ion-exchange capacity (like in zeolites) make them attractive in catalysis.<sup>22</sup> Due to their high hydrothermal stability,<sup>23</sup> they have been used as catalysts and supports in biomass transformation.<sup>24-30</sup> Pt supported on metal phosphates exhibited high activity for the hydrogenolysis of glycerol to 1- and 2-propanols (1- and 2-POs) with a yield of 97% at 220 °C and atmospheric pressure in a fixed-bed reactor.<sup>31</sup> As the combination of Pt and W exhibits high selectivity toward

Catalysis and Inorganic Chemistry Division, CSIR-National Chemical Laboratory, Dr Homi Bhabha Road, Pune-411008, India. E-mail: [d.srinivas@ncl.res.in](mailto:d.srinivas@ncl.res.in);  
Fax: +91-20-25902633; Tel: +91-20-25902018

† Electronic supplementary information (ESI) available: Catalytic activity calculation, XRD profiles and nitrogen physisorption data. See DOI: 10.1039/d0nj05557c

1,3-PDO, in this study, we have attempted this combination on ZrP and probed the hydrogenolysis reaction of aqueous glycerol at a moderate temperature (200 °C). Additionally, we report the application of proton nuclear magnetic resonance (<sup>1</sup>H NMR) spectroscopy – solvent suppression pulse program for identification and quantification of glycerol hydrogenolysis products. The product analysis is conventionally carried out by chromatographic methods. The NMR method is a simple and non-destructive tool and opens up an opportunity for this reaction as a characterization tool. While our work was in progress, Luo *et al.*<sup>32</sup> reported a study using a similar catalyst (Pt/7WO<sub>x</sub>-ZrP) that resulted mainly in 1-PO (81% yield) in a continuous flow reaction conducted at a higher temperature (270 °C). Our study reports the catalyst behavior at lower temperatures and we observe formation of PDOs as a major product.

## 2 Experimental section

### 2.1 Catalyst preparation

**2.1.1 ZrP.** In a typical synthesis of ZrP by a hydrothermal method,<sup>33</sup> 100 ml of Milli-Q water was taken in a beaker (250 ml capacity), and 3.9246 g of orthophosphoric acid (85 wt%, Thomas Baker) was added drop-wise with constant stirring. Then, 6.5572 g of zirconium isopropoxide (70 wt% solution in 1-PO, Sigma-Aldrich) was added to it. The mixture was stirred for 2 h at 25 °C and transferred into a Teflon-lined stainless steel autoclave (200 ml capacity). It was placed in an air-oven and aged statically at 80 °C for 24 h. The solid ZrP formed was filtered, dried overnight at 110 °C, ground into a fine powder and used in further study.

**2.1.2 Pt/ZrP.** ZrP-supported Pt catalysts (Pt = 1 and 2 wt%) were prepared by a wet impregnation method using tetraammineplatinum(II) nitrate (99.99%, Sigma-Aldrich) as a Pt source. A required amount of the Pt source was dissolved in 10 ml of Milli-Q water. To it, ZrP (1 g, prepared as above) was added and the suspension was stirred at 40 °C for 4 h. Then, water in it was removed over a rotary evaporator. The solid formed was recovered, dried overnight at 110 °C, and calcined in a muffle furnace at 450 °C for 4 h (ramp rate = 2 °C min<sup>-1</sup>). It was reduced in a flow of hydrogen (50 ml min<sup>-1</sup>) at 350 °C for 2.5 h (ramp rate = 10 °C min<sup>-1</sup>). The catalyst, thus obtained, was labeled as *x*Pt/ZrP. Here '*x*' refers to the nominal Pt content (wt%) in the catalyst.

**2.1.3 Pt/WO<sub>x</sub>/ZrP.** A series of bimetallic Pt/WO<sub>3</sub>/ZrP catalysts (Pt = 1 and 2 wt%, and *W* = 2, 4, 8, 12 and 16 wt%) was prepared by a sequential wet impregnation method. Firstly, the W source was impregnated on ZrP and then, the Pt source was impregnated. In the first-step, while stirring, a required amount of ammonium metatungstate ((NH<sub>4</sub>)<sub>6</sub>H<sub>2</sub>W<sub>12</sub>O<sub>40</sub>·*n*H<sub>2</sub>O – W source, Sigma-Aldrich) was dissolved in 10 ml of Milli-Q water taken in a glass round-bottom flask (100 ml capacity) placed in a temperature-controlled oil bath maintained at 40 °C. To it, 1 g of ZrP powder was added and the suspension was stirred for 16 h while heating at 40 °C. Then, water in it was removed over a rotary evaporator. The solid formed was dried in an oven overnight at 110 °C and calcined at

450 °C for 4 h (ramp rate = 2 °C min<sup>-1</sup>). The sample obtained was named as *y*WO<sub>3</sub>/ZrP, where *y* was the nominal weight percentage of tungsten in the sample.

Then, in the second-step, the required amount of tetraammine-platinum(II) nitrate (Pt source) was dissolved in 10 ml of Milli-Q water. *y*WO<sub>3</sub>/ZrP (1 g) was added to it. The suspension was stirred at 40 °C for 4 h. Water in it was removed by using a rotary evaporator. The solid formed was dried and calcined as described above. Then, it was reduced in a flow of hydrogen (50 ml min<sup>-1</sup>) at 350 °C for 2.5 h (ramp rate = 10 °C min<sup>-1</sup>). This catalyst was labeled as *x*Pt/*y*WO<sub>3</sub>/ZrP. Here, *x* is the nominal weight percentage of Pt and *y* is the weight percentage of *W* in the catalyst.

### 2.2 Catalyst characterization techniques

Structural characteristics of the catalyst samples were determined by X-ray powder diffraction (XRD) performed using a PANalytical X'Pert Pro diffractometer with a dual goniometer, X'celerator solid-state detector module and Ni-filtered Cu-K<sub>α</sub> radiation (λ = 0.15418 nm) operating at 40 kV and 30 mA. The diffraction data were collected between the incident angles of 2θ = 5° and 90° at a scan rate of 1.416° min<sup>-1</sup>. Textural properties of the samples were deduced from nitrogen-physorption studies conducted on an Autosorb-1C Quantachrome, USA instrument. Prior to nitrogen adsorption (at -196 °C), the catalyst samples were pretreated by degassing at 350 °C for 3 h. The Brunauer–Emmett–Teller specific surface area (*S*<sub>BET</sub>) of the catalysts was calculated from six adsorption data points in the relative pressure (*P*/*P*<sub>0</sub>) region of 0.05 ≤ *P*/*P*<sub>0</sub> ≤ 0.3 of the isotherm. Pore volume (PV) of the catalyst sample was calculated following the Barrett–Joyner–Halenda (BJH) method. Microstructural analysis of the catalyst samples was done by transmission electron microscopy (TEM) performed on a JEM-F200 multi-purpose electron microscope (JEOL Ltd) fitted with a 200 kV field emission gun. 0.001–0.005 g of the sample was suspended in 5 ml of 2-PO. It was sonicated for 30 min at 25 °C and a drop of this suspension was placed on a copper grid (200 mesh, ICON Analytical) and allowed to dry before it was subjected to the TEM analysis.

Fourier transform Raman (FT-Raman) spectra were recorded on a Horiba-Jobin-Yvon LabRAM HR 800 spectrometer. The spectra were acquired using a 632 nm (He–Ne) laser (20 mW) with an acquisition time of 10 s. The FT-Raman spectra were recorded in the wave number region of 200–1600 cm<sup>-1</sup>. Diffuse reflectance UV-visible (DRUV-vis) spectroscopy measurements were conducted on a Shimadzu UV-2700 spectrophotometer equipped with an integrating sphere attachment. The spectra were recorded in the wavelength range of 200 to 800 nm. The Kubelka–Munk (*K. M.*) function (*F*(*R*<sub>∞</sub>)) for infinitely thick samples was used to convert reflectance measurements (*R*<sub>Sample</sub>) into equivalent absorption spectra using the reflectance of BaSO<sub>4</sub> as a reference standard (*R*<sub>Standard</sub>) and the following equation:

$$F(R_{\infty}) = \frac{(1 - R_{\infty})^2}{2R_{\infty}} = \frac{\alpha(\text{absorption coefficient})}{S(\text{scattering coefficient})}$$

where,

$$R_{\infty} = \frac{R_{\text{Sample}}}{R_{\text{Standard}}}$$

### 2.3 Reaction procedure: hydrogenolysis of glycerol

The hydrogenolysis reaction of glycerol was conducted in a 100 ml batch stainless steel pressure reactor. In a typical reaction, 0.1 g of glycerol (Sigma-Aldrich) and 3 g of Milli-Q water were taken in the reactor. 0.1 g of the catalyst was added to it. The reactor was sealed, purged with nitrogen to expel out the air present inside the reactor and then, pressurized with hydrogen to 40 bar. The temperature was raised to 200 °C and the reaction was conducted for 6 to 12 h while stirring (500 rpm). Later, the reactor was cooled down to 25 °C. The gas was vented out and the reaction mixture was collected. About 1 ml of Milli-Q water was added additionally to the reactor vessel and any left out content was taken out and combined with the other amount. The catalyst was separated by centrifugation/filtration. Then, the liquid was passed through an MS<sup>®</sup> Nylon Syringe Filter (diameter = 33 mm and pore size = 0.22 μm) to eliminate any catalyst particles in it and then, analyzed by <sup>1</sup>H NMR spectroscopy. For comparison a few products were analyzed also by high performance liquid chromatography (HPLC). Each reaction and analyses were repeated thrice to confirm the reproducibility.

### 2.4 Product analysis

**2.4.1 <sup>1</sup>H NMR.** To date chromatographic techniques are used to monitor the reaction of glycerol hydrogenolysis. We report, here, a <sup>1</sup>H NMR spectroscopy method to monitor and quantify this reaction. The <sup>1</sup>H NMR method is simple, quick and non-destructive to analyze the products of this reaction. It is used for quantitative analysis because of the fact that the intensity of the NMR signal is proportional to the content as well as the number of proton nuclei of the product molecule. The error in estimation by this method is below 0.5%. The chromatographic methods require determination of response factors of each component which the NMR method doesn't demand. As the glycerol hydrogenolysis reaction is conducted in an aqueous medium, the GC method requires a special column for the analysis. NMR was applied for the quantitative analysis of glycerol in drug injections and several natural products such as food products, plant and herbal remedies and bio-fluids.<sup>34–36</sup> Vila *et al.*<sup>37</sup> used standard <sup>1</sup>H NMR and Zyu *et al.*<sup>38</sup> employed diffusion-ordered spectroscopy (DOSY), a pseudo two-dimensional (2D) NMR technique and 1D selective total correlation spectroscopy (TOCSY) to identify the glycerol hydrogenolysis products.

In the present study, the <sup>1</sup>H NMR spectra were recorded on a Bruker AV400 spectrometer. To about 0.025 g of the hydrogenolysis product, 0.6 ml of D<sub>2</sub>O (for external locking purpose; Sigma-Aldrich) was added and used in the analysis. A simple and robust solvent (H<sub>2</sub>O)-suppression program (*zgpr* – 1D water pre-saturation) that enabled acquisition of high quality <sup>1</sup>H NMR spectra of the reactant and products was adopted

(Fig. 1). In this program, a low power continuous wave (CW) irradiation (presat, p19) on the solvent (H<sub>2</sub>O) was applied before the first 30° <sup>1</sup>H pulse (p1) during the relaxation delay (d1). A normal method of <sup>1</sup>H NMR analysis (using standard *zg30* program) is not suitable as the solvent signal is much more intense than the spectral features of glycerol and product molecules and it thereby, presents a poor quality (low intensity) spectrum that is not suitable for analysis and quantification. Representative <sup>1</sup>H NMR spectra of an aqueous solution of glycerol before (c and d) and after the hydrogenolysis reaction (e and f) over the 1Pt-8WO<sub>x</sub>/ZrP catalyst with normal (a) and solvent-suppression (b) pulse sequences are shown in Fig. 1. The assignments of the <sup>1</sup>H NMR signals of glycerol and its products are presented in Table 1. The signals due to 1,2- and 1,3-PDOs were clearly separated in the <sup>1</sup>H NMR spectrum enabling quantification of their individual selectivity. The following parameters were employed in acquiring the <sup>1</sup>H NMR spectra: p1 = 13.24 μs (for 90° high power pulse), plw1 = 11.00 W, plw9 = 0.00005617 W (only in the case of *zgpr*), spectral width (SWH) = 8196.722 Hz, acquisition time (AQ) = 3.9976959 s, receiver gain (RG) = 43.4783 number of scans (NS) = 16 (for *zg30*) and 32 (for *zgpr*), dummy scans (DS) = 2, display number of points used to define FID (TD) = 65536, relaxation delay (d1) = 1.0 s, DW = 61.0 μs, and DE = 12.99 μs (for *zg30*) and 10.16 μs (for *zgpr*). Product selectivity (mol%) was determined from the areas of the <sup>1</sup>H NMR signals of the product components. In this calculation the NMR signals of glycerol appearing at 3.65–3.77 ppm (due to –CH<sub>c</sub>(OH); 1H; multiplet), 1,3-PDO at 1.68–1.72 ppm (–CH<sub>b</sub>–; 2H; multiplet), 1,2-PDO at 1.04–1.05 ppm (–CH<sub>d</sub>; 3H; doublet), 1-PO at 0.79–0.82 ppm (–CH<sub>a</sub>; 3H; triplet) and 2-PO at 1.08–1.09 ppm (–2CH<sub>2</sub>; 6H; doublet) were considered (Fig. 1 and Table 1). The following equations were used to estimate the percentage glycerol conversion, distribution of chemical component and component selectivity from the <sup>1</sup>H NMR spectra. An example of the calculation for 1Pt-8WO<sub>3</sub>/ZrP is reported in the ESI† (S1).

$$\begin{aligned} \text{Distribution of component Xi (mol\%)} \\ &= \frac{\text{Area of the peak of Xi (normalized to one proton)}}{\sum_{i=1}^n \text{Area of peak of Xi (normalized to one proton)}} \times 100 \end{aligned}$$

Glycerol conversion (mol%) = 100 – Percentage distribution of glycerol in the reaction mixture

Selectivity of product Xi (mol%)

$$= \frac{\text{Percentage distribution of Xi in the product}}{\text{Percentage of glycerol conversion}} \times 100$$

**2.4.2 HPLC.** A PerkinElmer (Series 200) HPLC equipped with a refractive index detector (PerkinElmer Series 400) was used. Product separation was achieved using a REZEX ROA (H<sup>+</sup> Organic Acid) column. 0.005 M H<sub>2</sub>SO<sub>4</sub> was used as the mobile phase at a flow rate of 0.5 ml min<sup>-1</sup>. The column

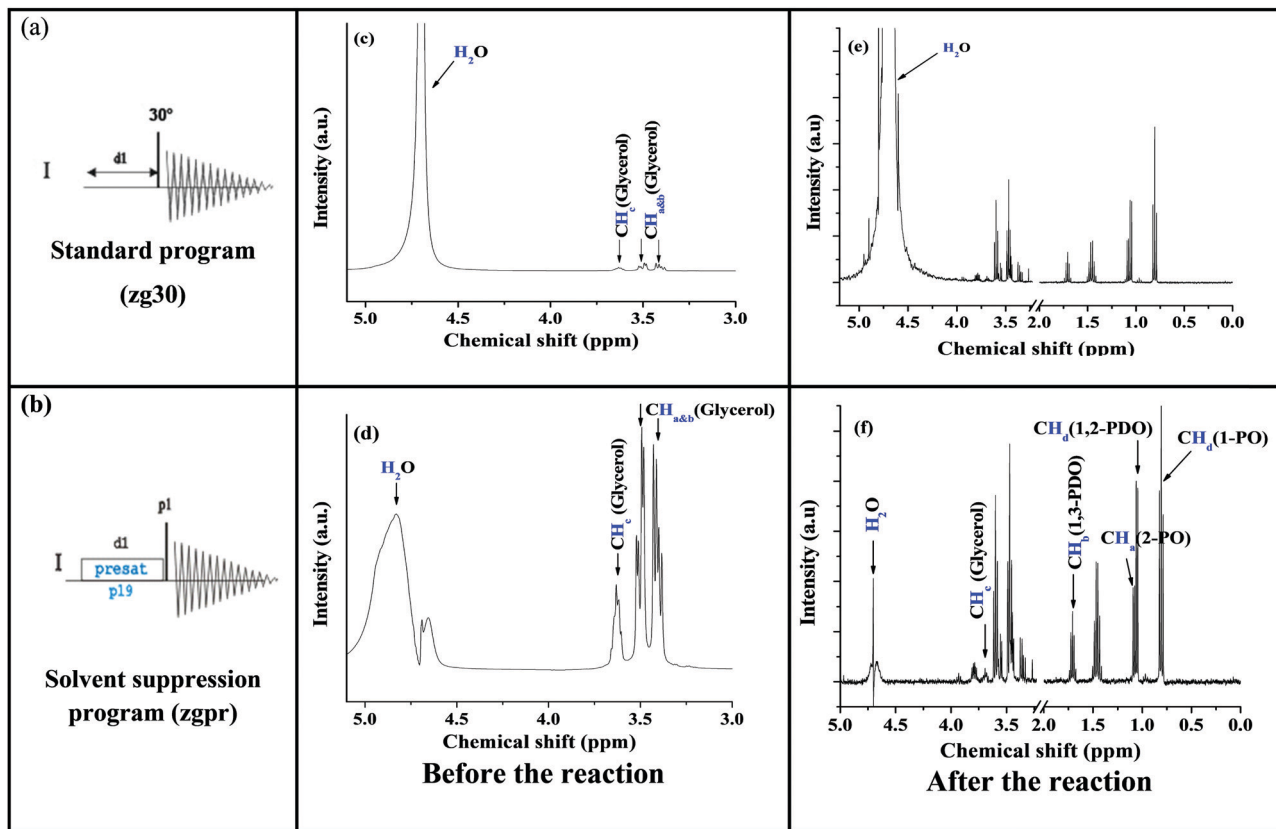


Fig. 1  $^1\text{H}$  NMR pulse programs for (a) standard (zg30) and (b) solvent suppression (zgpr) experiments. Standard  $^1\text{H}$  NMR spectra of aqueous glycerol solution: (c) before and (e) after the hydrogenolysis reaction. Solvent suppressed  $^1\text{H}$  NMR spectra of the above solution: (d) before and (f) after the reaction. Reaction conditions: glycerol (0.1 g), water (3 g), catalyst – 1Pt/8WO<sub>3</sub>/ZrP (0.1 g), hydrogen pressure at 25 °C = 40 bar, reaction temperature = 200 °C and reaction time = 12 h.

temperature was maintained at 60 °C throughout the HPLC analysis and a typical analysis run lasted for about 40 min. Product identification was carried out by using standard samples. The retention times of the HPLC peaks of the reactant

Table 1 Assignment of  $^1\text{H}$  NMR peaks of glycerol and its hydrogenolysis products

Compound	Molecular structure	Proton chemical shift (ppm)	Spectral pattern
Glycerol		<b>H<sub>a</sub></b> : 3.54–3.63 <b>H<sub>b</sub></b> : 3.54–3.63 <b>H<sub>c</sub></b> : 3.65–3.77	Doublet of doublet Doublet of doublet Multiplet
1,3-Propanediol (1,3-PDO)		<b>H<sub>a</sub></b> : 3.60 <b>H<sub>b</sub></b> : 1.68–1.72	Triplet Multiplet
1,2-Propanediol (1,2-PDO)		<b>H<sub>a</sub></b> : 3.44–3.52 <b>H<sub>b</sub></b> : 3.44–3.52 <b>H<sub>c</sub></b> : 3.86 <b>H<sub>d</sub></b> : 1.04–1.05	Doublet of doublet Doublet of doublet Multiplet Doublet
1-Propanol (1-PO)		<b>H<sub>a</sub></b> : 3.59 <b>H<sub>b</sub></b> : 3.59 <b>H<sub>c</sub></b> : 1.59 <b>H<sub>d</sub></b> : 0.79–0.82	Doublet of triplet Doublet of triplet Multiplet Triplet
2-Propanol (2-PO)		<b>H<sub>a</sub></b> : 1.08–1.09 <b>H<sub>b</sub></b> : 4.0	Doublet Septet

and products were as follows: glycerol (16.9 min), ethylene glycol (EG, 19.9 min), 1,2-propanediol (1,2-PDO, 21.2 min), 1,3-propanediol (1,3-PDO, 21.6 min), ethanol (26.4 min), 2-propanol (2-PO, 29.0 min) and 1-propanol (1-PO, 32.5 min). In most cases, the peaks of diols (1,2- and 1,3-PDO) overlapped and appeared as a partially split peak with maximum at around 21.4 min. Hence, we didn't quantify separately the selectivity of 1,2- and 1,3-PDO from the HPLC analysis. It is reported only as total diol (1,2- + 1,3-PDO) selectivity. The following formulae were used to calculate glycerol conversion and product selectivity (wt%) from the HPLC analysis.

Glycerol conversion (%) =

$$\frac{(\text{Area of glycerol peak at zero time} - \text{Area of glycerol peak at time } t)}{\text{Area of glycerol peak at zero time}}$$

× 100

Product selectivity (%)

$$= \frac{\text{Area of product peak at time } t}{\text{Sum of the areas of all products peaks at time } t} \times 100$$

## 3 Results and discussion

### 3.1 Catalyst characterization

"Neat" ZrP showed two broad XRD peaks in the  $2\theta$  ranges of  $10\text{--}40^\circ$  and  $40\text{--}70^\circ$  asserting its amorphous structure (ESI,† S2).<sup>31</sup> A tungsten loaded sample ( $8\text{WO}_3/\text{ZrP}$ ) showed additional sharp peaks at  $2\theta = 23.2, 23.8, 26.6, 28.8, 33.5$  and  $34.0^\circ$  assignable to (002), (020), (120), (112), (022) and (202) planes, respectively, of monoclinic (I)  $\gamma\text{-WO}_3$  phase (COD 2106382).<sup>39</sup>  $2\text{Pt}/\text{ZrP}$  exhibited a pattern similar to "neat" ZrP. No peaks due to metallic Pt were detected implying that Pt crystallites in this sample are highly dispersed on the ZrP surface and their crystal size is below the X-ray detection limit. The bimetallic composition,  $2\text{Pt}/8\text{WO}_3/\text{ZrP}$  depicted a profile containing the XRD patterns of both ZrP and  $\gamma\text{-WO}_3$  and additional peaks (at  $2\theta = 39.6, 46.1, 67.4$  and  $81.5^\circ$  due to the (111), (200), (220) and (311) planes, respectively) of metallic Pt having a cubic close-packed structure (with space group of  $Fm\bar{3}m$ ; JCPDS No. 65-2868) (ESI,† S2). TEM studies validated the highly dispersed nature of Pt particles on ZrP (Fig. 2). The average particle size of Pt (determined from 100 random particles) was 1.5–2.0 nm for

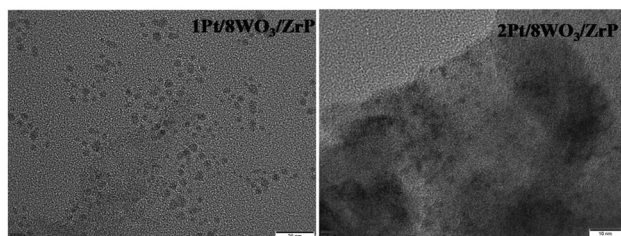


Fig. 2 TEM images of  $1\text{Pt}/8\text{WO}_3/\text{ZrP}$  (left) and  $2\text{Pt}/8\text{WO}_3/\text{ZrP}$  (right).

$1\text{Pt}/8\text{WO}_3/\text{ZrP}$  and  $2\text{Pt}/8\text{WO}_3/\text{ZrP}$  and it was smaller for mono-metallic Pt/ZrP samples.

The  $\text{N}_2$  adsorption–desorption isotherms of ZrP samples (ESI,† S3) were of type II behavior, characteristic of layered materials.<sup>40</sup> These isotherms should not be confused with type IV isotherms as they don't have a plateau at high relative pressure ( $P/P_0$ ) values. Hysteresis loops ( $\text{H}_3$  type) were observed at relative pressures where multi-layers and capillary condensation occur. These loops closed at  $P/P_0$  values in the range of 0.2 to 0.4 depending on the catalyst composition and represent the solids with wide distribution of pore sizes. This pseudo-type II character of the physisorption isotherms corresponded to the meta-stability of the adsorbed multilayer and delayed capillary condensation due to a low-degree of pore curvature and non-rigidity of the aggregate structure. The shape of the  $\text{H}_3$  loop was linked to the non-rigid nature of the adsorbent and slit-shaped pores.<sup>41</sup> The specific surface area ( $S_{\text{BET}} = 13\text{--}29 \text{ m}^2 \text{ g}^{-1}$ ) and pore volume ( $0.04\text{--}0.10 \text{ ml g}^{-1}$ ) of the samples were found to be low (ESI,† S4) corresponding to the amorphous nature of the ZrP samples. The average pore radius of the samples was in the range of 1.7 to 2.1 nm.

DRUV-vis spectroscopy is a useful technique to probe the electronic structure and domain size of transition metal oxides. "Neat" ZrP showed a weak band in the DRUV-vis spectrum (Fig. 3(a)) with maximum at 278 nm due to ligand-to-metal charge transfer (LMCT) transition (phosphate oxygen ions to zirconium cations;  $\text{O}^{2-} \rightarrow \text{Zr}^{4+}$ ). This band for  $\text{Pt}\text{-WO}_3/\text{ZrO}_2$  was reported to occur at 230 nm.<sup>42</sup> Phosphate ions (instead of neat  $\text{O}^{2-}$ ) in the structure could be the reason for the red-shift of the LMCT band in the ZrP samples.  $8\text{WO}_3/\text{ZrP}$  and  $2\text{Pt}/8\text{WO}_3/\text{ZrP}$  showed absorptions (spread over the spectral range of 200–450 nm) that could be deconvoluted into three bands with peak maximum at 220, 260 and 340 nm (Fig. 3(a)). These bands were attributed to oxygen ( $\text{O}_{2p}$ ) to tungsten ( $\text{W}_{5d}$ ) charge transfer transitions in the tungsten oxide species of the samples.<sup>43</sup> Guntida *et al.*,<sup>44</sup> in their studies on  $\text{SiO}_2$  and  $\text{Al}_2\text{O}_3$ -supported tungsten found three types of tungsten species *viz.*, tetrahedral  $\text{WO}_3$ , octahedral polytungstate and crystalline  $\text{WO}_3$  species. The two high energy UV bands at 220 and 260 nm may be assigned to the tungsten species with distorted tetrahedral and octahedral coordination environments, respectively,

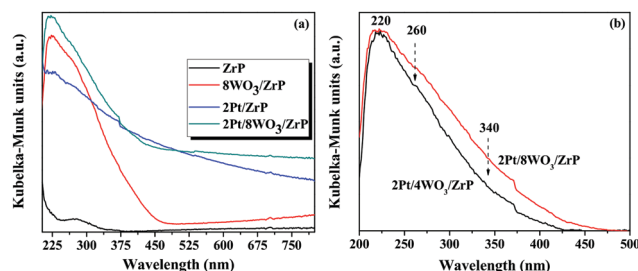


Fig. 3 (a) Diffuse reflectance UV-visible spectra of ZrP,  $8\text{WO}_3/\text{ZrP}$ ,  $2\text{Pt}/\text{ZrP}$  and  $2\text{Pt}/8\text{WO}_3/\text{ZrP}$ . (b) Comparative spectra of  $2\text{Pt}/4\text{WO}_3/\text{ZrP}$  and  $2\text{Pt}/8\text{WO}_3/\text{ZrP}$  under normalized conditions. Spectral bands due to isolated monomeric  $\text{WO}_3$  (220 nm), polytungstate clusters (260 nm) and crystalline  $\text{WO}_3$  (340 nm) are marked.

while the lower energy band at 340 nm corresponded to the crystalline  $\text{WO}_3$  species. Pt/ZrP showed a broad background absorption in the measured spectral range due to Pt being in the metallic state.

The surface densities of W atoms for 4 and 8 wt% W catalysts (calculated using  $S_{\text{BET}}$  values) were 4.5 and 14.6  $\text{W nm}^{-2}$ , respectively. Barton *et al.*<sup>45</sup> demonstrated the tungsten density of 0–4  $\text{W nm}^{-2}$  as the sub-monolayer region (where isolated four-coordinate  $\text{W}^{6+}$  centers tetrahedrally coordinated to oxygen showing the highest absorption edge energy value of 4.89 eV and difficult to reduce with hydrogen species exist), 4–8  $\text{W nm}^{-2}$  as the polytungstate growth region (where isolated polytungstate clusters containing tungsten oxide octahedra bonded through corner and edges, showing intermediate absorption edge energy values of about 3.54 eV and easier to reduce species exist), and  $>8 \text{ W nm}^{-2}$  as the polytungstate/crystalline  $\text{WO}_3$  coexistence region (where  $\text{WO}_x$  species in an extended three-dimensional crystalline network of distorted tungsten oxide octahedra bonded to six neighboring tungsten oxide octahedra showing lowest absorption edge energies of 2.59 eV and the easiest to reduce exist). Thus, in the ZrP samples with 4 wt% W (surface density = 4.5  $\text{W nm}^{-2}$ ), the tungsten oxide species are mainly in polytungstate form, and in the samples with 8 wt% W (surface density = 14.6  $\text{W nm}^{-2}$ ), polytungstate combined with crystalline  $\text{WO}_3$  are the prevalent W species. Comparative DR UV-vis spectra under normalized conditions (Fig. 3(b)) have indeed revealed this conclusion by exhibiting more intense 260 and 340 nm bands in 2Pt-8 $\text{WO}_3$ /ZrP than in 2Pt-4 $\text{WO}_3$ /ZrP. XRD studies (ESI,† S2) have also authenticated this conclusion showing the characteristic peaks for the presence of crystalline, monoclinic  $\text{WO}_3$  species in 8 $\text{WO}_3$ /ZrP and 2Pt-8 $\text{WO}_3$ /ZrP samples.

FT-Raman spectroscopy is a valuable technique for unraveling the molecular structure of metal oxides. “Neat” ZrP showed a characteristic Raman band at 1055  $\text{cm}^{-1}$  attributable to P–O vibrations in the orthophosphate group ( $\text{HPO}_4^{2-}$ ).<sup>45</sup> On loading Pt, a shift in the position of this vibrational band to a higher value (1072  $\text{cm}^{-1}$ ) was observed, indicating strong interaction of supported Pt particles with the orthophosphate moiety of ZrP. A weak, additional vibrational feature was observed at 230  $\text{cm}^{-1}$  for 2Pt/ZrP corresponding to the support. FT-Raman spectra of some representative  $x\text{Pt}/y\text{WO}_3$ /ZrP samples are pictured in Fig. 4 and 5. In these samples, additional spectral features due to the presence of tungsten oxide were observed. The position and intensity of these Raman bands varied with the W content. 1Pt/2 $\text{WO}_3$ /ZrP showed an intense band at 1013  $\text{cm}^{-1}$  and a weak band at 428  $\text{cm}^{-1}$ .

These have been assigned to the symmetric stretching mode of terminal  $\text{W}=\text{O}$  and  $\text{W}-\text{O}$  bonds, respectively, present in isolated, tetrahedral monotungstate and octahedral polytungstate cluster species and at the surface of  $\text{WO}_3$  crystals.<sup>45</sup> A shift in the position of the Raman band of the support to 1078  $\text{cm}^{-1}$  due to interaction of  $\text{WO}_3$  with the support was noted. Strong interaction of  $\text{WO}_3$ , withdraws electron density from the orthophosphate moiety, strengthens the P–O bond and thereby leads to a high energy shift in the Raman band position.

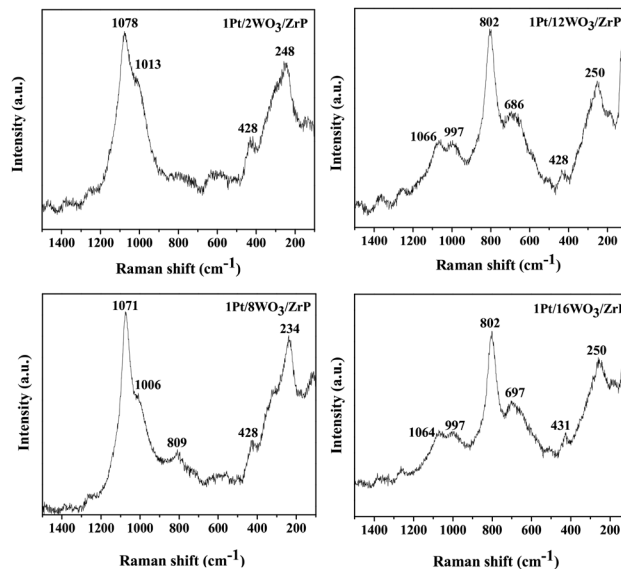


Fig. 4 FT-Raman spectra of  $x\text{Pt}/y\text{WO}_3$ /ZrP ( $x = 1$  and  $y = 2, 8, 12$  and  $16$ ). Raman bands of ZrP and polytungstate/crystalline  $\text{WO}_3$  are marked.

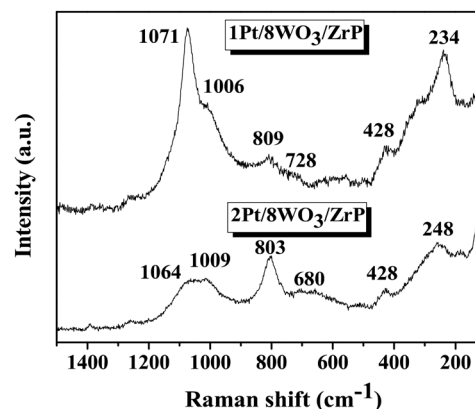
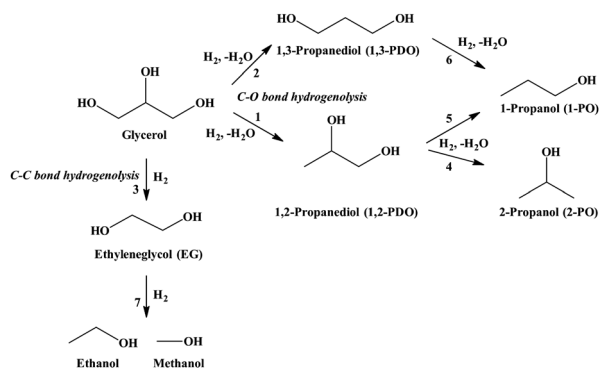


Fig. 5 FT-Raman spectra of 1Pt/8 $\text{WO}_3$ /ZrP and 2Pt/8 $\text{WO}_3$ /ZrP.

With increasing tungsten amount (from 2 to 16 wt%), a growth in the intensity of the peaks at 809, 686 and 248  $\text{cm}^{-1}$  corresponding to W–O stretching, W–O bending and W–O–W deformation modes, respectively, of crystalline  $\text{WO}_3$  was observed (Fig. 4).<sup>20</sup> In conformity with DRUV-vis and XRD results, FT-Raman spectroscopy concludes that the catalyst with 8 wt% W contains both polytungstate and crystalline  $\text{WO}_3$  species, with the former being more abundant than the latter type tungsten oxide species. The samples with 12 and 16 wt% W contained more proportion of crystalline  $\text{WO}_3$  species (intense Raman features at 809 and 686  $\text{cm}^{-1}$ ). A shift in the Raman band position to lower wave numbers with increasing W content was detected confirming the growth in the grain size of the  $\text{WO}_3$  species.<sup>46</sup> Also Pt content had an effect on the type of  $\text{WO}_3$  species in the bimetallic catalysts (Fig. 5). While maintaining the W content at 8 wt%, the Pt content was varied from 1 to 2 wt%. It was found from the



Scheme 1 C–O and C–C bond hydrogenolysis products of glycerol.<sup>10</sup>

FT-Raman spectral intensity ( $I_{809}/I_{1071}$ ) and band positions that the relative amount of crystalline  $\text{WO}_3$  (as against the polytungstate species) and grain size of tungsten species were higher in 2Pt/8 $\text{WO}_3$ /ZrP than in 1Pt/8 $\text{WO}_3$ /ZrP. Thus, the amounts of Pt and W control the interaction and structure of metal species present on the ZrP surface.

### 3.2. Catalytic activity

Glycerol can undergo hydrogenolysis at its C–O and C–C bond positions (Scheme 1; eqn (1)–(7)). While the hydrogenolysis of the primary C–O bond yields 1,2-propanediol (1,2-PDO; 1), that of the secondary C–O bond produces 1,3-propanediol (1,3-PDO; 2).

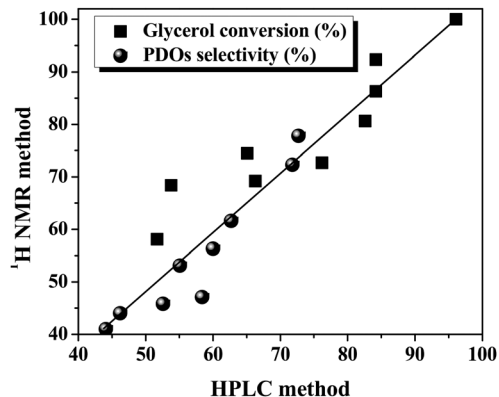


Fig. 6 Correlation plot of glycerol conversion and PDO selectivity obtained from HPLC and  $^1\text{H}$  NMR analyses. The  $R^2$  values for glycerol conversion and PDO selectivity were 0.895 and 0.842, respectively.

Table 2 Hydrogenolysis of glycerol over mono and bimetallic ZrP-supported Pt catalysts<sup>a</sup>

Catalyst	Glycerol conversion (%)	Product selectivity (%), $^1\text{H}$ NMR				$\frac{1,3\text{-PDO}}{1,2\text{-PDO}}$	TOF ( $\text{h}^{-1}$ )
		1,3-PDO	1,2-PDO	1-PO	2-PO		
1Pt/ZrP	37.5	16.7	55.6	22.2	5.5	0.3	7
2Pt/ZrP	69.2	11.1	66.7	22.2	0	0.2	6
1Pt/8 $\text{WO}_3$ /ZrP	92.3	20.9	25.0	47.2	6.9	0.8	16
2Pt/8 $\text{WO}_3$ /ZrP	68.4	23.1	38.5	34.6	3.8	0.6	6

<sup>a</sup> Reaction conditions: Glycerol = 0.1 g, water = 3 g, catalyst = 0.1 g, hydrogen pressure = 40 bar, reaction temperature = 200 °C and reaction time = 12 h. 1,2-PDO = 1,2-propanediol, 1,3-PDO = 1,3-propanediol, 1-PO = 1-propanol and 2-PO = 2-propanol. Turnover frequency (TOF) = moles of glycerol converted per mole of Pt per hour.

A further reaction of 1,2-PDO gives 1- and 2-propanols (1- and 2-POs; 4 and 5) and that of 1,3-PDO gives 1-PO (6). On the other hand, the C–C bond hydrogenolysis of glycerol yields ethyleneglycol (EG) (3), and its further reaction forms ethanol and methanol (7). All these hydrogenolysis products of glycerol are liquids under ambient conditions. Reduction of mono alcohols yields gaseous (C1–C3) hydrocarbon products. The yield of the liquid products in the reactions over ZrP catalysts was nearly 98% of the theoretical value suggesting that over-reduction to hydrocarbons (to gaseous products) was insignificant at our reaction conditions and hence, they were neglected.

Unlike chromatographic techniques,  $^1\text{H}$  NMR spectroscopy avoids the need of determining response factors of reactant and product molecules. As solvent-water shows a dominant  $^1\text{H}$  NMR signal causing trouble in the product analysis (as the peaks of the products appear less intense than the solvent peak), we used one-dimensional, solvent-suppression  $^1\text{H}$  pulse-program in the analysis (Section 2.4.2; Fig. 1). Employing this technique, the solvent signal was saturated and its intensity was suppressed. Then, the peaks of glycerol and the products became prominent and quantifiable. The spectral features of 1,2- and 1,3-PDOs were resolved (see the signals in the regions of 1.04–1.05 ppm for 1,2-PDO and 1.68–1.72 ppm for 1,3-PDO; Fig. 1).  $^1\text{H}$  NMR enabled determination of their selectivity (Section 2.4.2). The NMR spectroscopy confirmed the formation of 1,2- and 1,3-PDOs and 1- and 2-POs in the reaction. Glycerol conversion and product selectivity variation trends of the catalysts determined by HPLC and  $^1\text{H}$  NMR were nearly the same (Fig. 6) and confirm that  $^1\text{H}$  NMR spectroscopy is a convenient and alternative analytical method to monitor the glycerol hydrogenolysis reaction.

Control experiments conducted at 200 °C and 40 bar  $\text{H}_2$  for 12 h in the presence of ‘neat’ ZrP and 8 $\text{WO}_3$ /ZrP showed no conversion of glycerol. 1Pt/ZrP enabled glycerol conversion of 37.5% confirming that Pt particles are the catalytic centers (Table 2). PDOs (1,3-PDO = 16.7% and 1,2-PDO = 55.6%) and 1-PO (22.2%) formed in higher amounts while 2-PO (5.5%) was the minor product. The results reveal that, over this catalyst, C–O bond hydrogenolysis (1 and 2) is the preferred reaction pathway rather than C–C bond hydrogenolysis (3). 1-PO is formed from both 1,2- and 1,3-PDOs (5 and 6), whereas 2-PO is formed only from 1,2-PDO (Scheme 1; reaction 4). The conversion of glycerol was higher (69.2%) when 2Pt/ZrP was used as the catalyst. However, the intrinsic catalytic activity

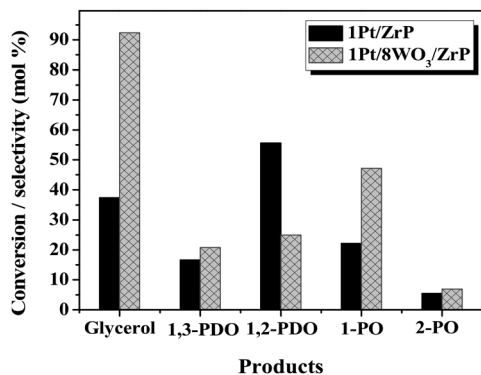


Fig. 7 Comparative glycerol hydrogenolysis activity of 1Pt/ZrP and 1Pt/8WO<sub>3</sub>/ZrP. Reaction conditions: same as in Table 2.

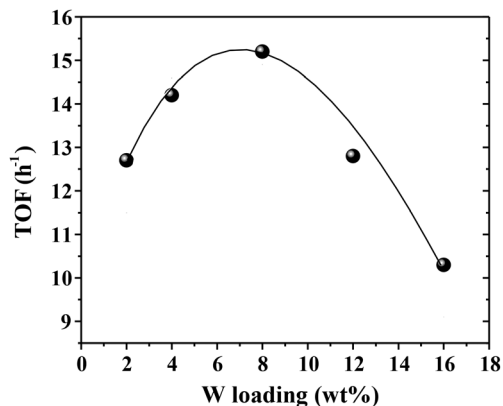


Fig. 8 Variation of TOF as a function of W loading in the hydrogenolysis of glycerol over Pt/WO<sub>3</sub>/ZrP,  $y = 2-16$  wt%. Reaction conditions: same as in Table 3.

(turnover frequency; TOF = moles of glycerol converted per mole of nominal Pt per hour) was about the same for both 1Pt/ZrP and 2Pt/ZrP (Table 2). A higher amount of active Pt with similar dispersion as in 1Pt/ZrP is the reason for the higher glycerol conversion over 2Pt/ZrP. In the reaction over a bimetallic 1Pt/8WO<sub>3</sub>/ZrP catalyst, a considerable increase in glycerol conversion (from 37.5% for 1Pt/ZrP to 92.3% for 1Pt/8WO<sub>3</sub>/ZrP) and 1,3-PDO selectivity (from 16.7 for 1Pt/ZrP to 20.9% for 1Pt/8WO<sub>3</sub>/ZrP) was detected (Fig. 7). TOF of Pt increased from 7 h<sup>-1</sup> (for 1Pt/ZrP) to 16 h<sup>-1</sup> (for 1Pt/8WO<sub>3</sub>/ZrP), inferring synergistic interaction between Pt and W species. The reaction to 1-PO was favored. The selectivity of total PDOs decreased from 72.3 to 45.9% and the selectivity of 1-PO increased from 22.2 to 47.2% (Table 2). Extent of over-hydrogenolysis to 1-PO was less prevalent on 2Pt/8WO<sub>3</sub>/ZrP than on 1Pt/8WO<sub>3</sub>/ZrP. FT-Raman study revealed a higher amount of crystalline WO<sub>3</sub> species (more intense 809 and 686 cm<sup>-1</sup> bands) in 2Pt/8WO<sub>3</sub>/ZrP than in 1Pt/8WO<sub>3</sub>/ZrP. The latter catalyst contained a higher proportion of polytungstate species. These differences in the WO<sub>3</sub> structures must be the cause for the difference in the hydrogenolysis selectivity observed over these bimetallic catalysts. The TOF values of 1Pt/ZrP and 2Pt/ZrP were nearly the same (7 and 6 h<sup>-1</sup>, respectively), but 1Pt/8WO<sub>3</sub>/ZrP showed much higher TOF (16 h<sup>-1</sup>) than 2Pt/8WO<sub>3</sub>/ZrP (6 h<sup>-1</sup>) indicating the influence of WO<sub>3</sub> structure on the activity of Pt. Furthermore, the particle size of Pt is slightly bigger on 2Pt/8WO<sub>3</sub>/ZrP (2 nm) than on 1Pt/8WO<sub>3</sub>/ZrP (1.5 nm, Fig. 2). These differences in the

structures of Pt and WO<sub>3</sub> are the probable cause for the lower catalytic activity of 2Pt/8WO<sub>3</sub>/ZrP than 1Pt/8WO<sub>3</sub>/ZrP.

Tungsten content in the bimetallic catalyst had a pronounced effect on glycerol conversion and 1,3-PDO selectivity. Having found that 1Pt/8WO<sub>3</sub>/ZrP is the active catalyst (TOF = 16 h<sup>-1</sup>), we varied the content of W in the catalyst from 2 to 16 wt% (Table 3). Catalytic activity (TOF) increased with increasing W content up to 8 wt% and then, decreased gradually above that. Fig. 8 demonstrates a *volcano-shape* variation of catalytic activity (TOF) with W content in the catalyst. 1Pt/8WO<sub>3</sub>/ZrP was found to be the most active catalyst with high selectivity to 1,3-PDO (Table 3). Highly dispersed nanoparticles of Pt in contact with polytungstate-like W-species are responsible for the highest activity of 1Pt/8WO<sub>3</sub>/ZrP. Such *volcano-shape* variations were reported also by others.<sup>15,47-49</sup> WO<sub>3</sub> acts as a promoter to the metal. Pt-(WO<sub>x</sub>)<sub>n</sub>-H with dispersed Pt metal and strong Brønsted acid adjacent to each other is the active catalytic center.<sup>20</sup> Bhanuchander *et al.*<sup>31</sup> using several metal phosphate (including ZrP)-supported Pt catalysts found 100% glycerol conversion with 97% selectivity to POs at 220 °C and atmospheric pressure. In our study, we show that by promoting with WO<sub>3</sub>, the selectivity to diols (in particular to 1,3-PDO) could be enhanced while suppressing the C-C bond cleavage and other product formation (Table 2). Although, high conversion of glycerol is achieved, the formation rate of 1,3-PDO over 1Pt/8WO<sub>3</sub>/ZrP is lower than the reported systems.<sup>12,13,15,42</sup> The reported catalysts contained a

Table 3 Effect of tungsten composition on the hydrogenolysis of glycerol over Pt/WO<sub>3</sub>/ZrP catalysts<sup>a</sup>

Catalyst	Glycerol conversion (%)	Product selectivity (%)				TOF (h <sup>-1</sup> )
		1,3-PDO	1,2-PDO	1-PO	2-PO	
1Pt/2WO <sub>3</sub> /ZrP	74.5	17.1	40.0	40.0	2.9	13
1Pt/4WO <sub>3</sub> /ZrP	80.6	12.0	32.0	48.0	8.0	14
1Pt/8WO <sub>3</sub> /ZrP	86.3	20.8	25.0	47.2	6.9	15
1Pt/12WO <sub>3</sub> /ZrP	72.7	18.8	37.5	37.5	6.2	13
1Pt/16WO <sub>3</sub> /ZrP	58.1	18.7	34.4	40.6	6.3	10
2Pt/4WO <sub>3</sub> /ZrP	100	15.4	25.6	51.3	7.7	9

<sup>a</sup> Reaction conditions: same as in Table 2.

higher amount of Pt (4–8 wt%) in their composition. To achieve higher productivity rate of 1,3-PDO, it is essential to enhance the surface area (by altering the synthesis procedure) and strong acidity of the catalyst, and also to suppress the over-hydrogenolysis activity (by introducing additives), which will be the study of our future work.

## 4 Conclusions

Bimetallic Pt/WO<sub>3</sub>/ZrP catalysts (prepared by the sequential wet impregnation method) exhibited high catalytic performance for the hydrogenolysis of glycerol in an aqueous medium. They gave mainly PDOs rather than POs at moderate temperatures (200 °C). Co-presence of Pt and W in the catalyst composition led to synergistic enhancement in the catalytic activity and 1,3-PDO selectivity. WO<sub>3</sub> promoted the product selectivity of Pt to diols (in particular to 1,3-PDO) rather than to other products. A volcano-shape variation of catalytic activity with the W content was found. A ZrP catalyst with 1 wt% Pt and 8 wt% W showed the best selective catalytic performance. Highly dispersed Pt nanoparticles in contact with polytungstate-like WO<sub>x</sub> species were active centers for the hydrogenolysis reaction. <sup>1</sup>H NMR spectroscopy was demonstrated as an alternative tool to chromatography to quantify the hydrogenolysis products.

## Conflicts of interest

There are no conflicts to declare.

## Acknowledgements

S. D. acknowledges the Council of Scientific and Industrial Research (CSIR), New Delhi for the award of a CSIR-Bhatnagar Fellowship (SSB 000926; P90807). The authors thank Dr Mrs Banu Marimuthu, Mr Sreejith Sreekantan, Ms Arun Arunima B. Kirali and Dr Uday Kiran Marelli for the support.

## Notes and references

- C.-H. Zhou, J. N. Beltramini, Y.-X. Fana and G. Q. Lu, *Chem. Soc. Rev.*, 2008, **37**, 527–549.
- J. ten Dam and U. Hanefeld, *ChemSusChem*, 2011, **4**, 1017–1034.
- D. Sun, Y. Yamada, S. Sato and W. Ueda, *Appl. Catal., B*, 2016, **193**, 75–92.
- M. R. Nanda, Z. Yuan, W. Qin and C. Xu, *Catal. Rev.: Sci. Eng.*, 2016, **58**, 309–336.
- M. R. Nimlos, S. J. Blanksby, X. Qian, M. E. Himmel and D. K. Johnson, *J. Phys. Chem. A*, 2006, **110**, 6145–6156.
- J. Oh, S. Dash and H. Lee, *Green Chem.*, 2011, **13**, 2004–2007.
- S. Bhowmik and S. Darbha, *Catal. Rev.: Sci. Eng.*, 2020, DOI: 10.1080/01614940.2020.1794737.
- Y. Nakagawa, Y. Shinmi, S. Koso and K. Tomishige, *J. Catal.*, 2010, **272**, 191–194.
- Y. Amada, Y. Shinmi, S. Koso, T. Kubota, Y. Nakagawa and K. Tomishige, *Appl. Catal., B*, 2011, **105**, 117–127.
- Y. Nakagawa, X. Ning, Y. Amada and K. Tomishige, *Appl. Catal., A*, 2012, **433–434**, 128–134.
- L. Liu, S. Kawakami, Y. Nakagawa, M. Tamura and K. Tomishige, *Appl. Catal., B*, 2019, **256**(Article No. 117775), 1–13.
- R. Arundhathi, T. Mizugaki, T. Mitsudome, K. Jitsukawa and K. Kaneda, *ChemSusChem*, 2013, **6**, 1345–1347.
- S. García-Fernández, I. Gandarias, Y. Tejido-Núñez, J. Requies and P. L. Arias, *ChemCatChem*, 2017, **9**, 4508–4519.
- S. Zhu, X. Gao, Y. Zhu and Y. Li, *J. Mol. Catal. A: Chem.*, 2015, **398**, 391–398.
- N. Lei, X. Zhao, B. Hou, M. Yang, M. Zhou, F. Liu, A. Wang and T. Zhang, *ChemCatChem*, 2019, **11**, 3903–3912.
- S. Zhu, X. Gao, Y. Zhu, J. Cui, H. Zheng and Y. Li, *Appl. Catal., B*, 2014, **158–159**, 391–399.
- S. Zhu, X. Gao, Y. Zhu, Y. Zhu, X. Xiang, C. Hu and Y. Li, *Appl. Catal., B*, 2013, **140–141**, 60–67.
- N. Lei, Z. Miao, F. Liu, H. Wang, X. Pan, A. Wang and T. Zhang, *Chin. J. Catal.*, 2020, **41**, 1261–1267.
- S. S. Priya, V. P. Kumar, M. L. Kantam, S. K. Bhargava, A. Srikanth and K. V. R. Chary, *Ind. Eng. Chem. Res.*, 2015, **54**, 9104–9115.
- W. Zhou, Y. Li, X. Wang, D. Yao, Y. Wang, S. Huang, W. Li, Y. Zhao, S. Wang and X. Ma, *J. Catal.*, 2020, **388**, 154–163.
- A. Clearfield and D. S. Thakur, *Appl. Catal.*, 1986, **26**, 1–26.
- M. Pica, *Catalysts*, 2017, 7(Article No. 190), 1–18.
- Y. Kamiya, S. Sakata, Y. Yoshinaga, R. Ohnishi and T. Okuhara, *Catal. Lett.*, 2004, **94**, 45–47.
- N. Li, G. A. Tompsett and G. W. Huber, *ChemSusChem*, 2010, **3**, 1154–1157.
- Y. T. Kim, J. A. Dumesic and G. W. Huber, *J. Catal.*, 2013, **304**, 72–85.
- G.-H. Han, M. W. Lee, S. Park, H. J. Kim, J.-P. Ahn and M.-G. Seo, *J. Catal.*, 2019, **377**, 343–357.
- C. Zhu, Q. Liu, D. Li, H. Wang, C. Zhang, C. Cui, L. Chen, C. Cai and L. Ma, *ACS Omega*, 2018, **3**, 7407–7417.
- Q.-Y. Liu, Y.-H. Liao, T.-J. Wang, C.-L. Cai, Q. Zhang, N. Tsubaki and L.-L. Ma, *Ind. Eng. Chem. Res.*, 2014, **53**, 12655–12664.
- G. Li, N. Li, Z. Wang, C. Li, A. Wang, X. Wang, Y. Cong and T. Zhang, *ChemSusChem*, 2012, **5**, 1958–1966.
- M. Wang, H. Yang, Y. Xie, X. Wu, C. Chen, W. Ma, Q. Dong and Z. Hou, *RSC Adv.*, 2016, **6**, 29769–29778.
- P. Bhanuchander, S. S. Priya, V. P. Kumar, S. Hussain, N. P. Rajan, S. K. Bhargava and K. V. R. Chary, *Catal. Lett.*, 2017, **147**, 845–855.
- R. Luo, X. Zhao, H. Gong, W. Qian, D. Li, M. Chen, K. Cui, J. Wang and Z. Hou, *Energy Fuels*, 2020, **34**, 8707–8717.
- T.-Z. Ren, Z.-Y. Yuan and B.-L. Su, *Chem. Commun.*, 2004, 2730–2731.
- J. Lu, P. Wang, Q. Wang, Y. Wang and M. Jiang, *Molecules*, 2018, **23**, 1177.
- M. Hohmann, V. Koospal, C. Bauer-Christoph, N. Christoph, H. Wachter, B. Diehl and U. Holzgrabe, *J. Agric. Food Chem.*, 2015, **63**, 4112–4119.

- 36 C. Simmler, J. G. Napolitano, J. B. McAlpine, S. N. Chen and G. F. Pauli, *Curr. Opin. Biotechnol.*, 2014, **25**, 51–59.
- 37 F. Vila, M. L. Granados and R. Mariscal, *Catal. Sci. Technol.*, 2017, **7**, 3119–3127.
- 38 Z. Lyu, F. Yue, X. Yan, J. Shan, D. Xiang, C. M. Pedersen, C. Li, Y. Wang and Y. Qiao, *Fuel Proc. Technol.*, 2018, **171**, 117–123.
- 39 K. Thummavichai, N. Wang, F. Xu, G. Rance, Y. Xia and Y. Zhu, *Roy. Soc. Open Sci.*, 2018, **5**(Art No. 171932), 1–10.
- 40 R. M. Barrer, *Pure Appl. Chem.*, 1989, **61**, 1903–1912.
- 41 K. S. W. Sing and R. T. Williams, *Adsorption Sci. Technol.*, 2004, **22**, 773–782.
- 42 Y. Fan, S. Cheng, H. Wang, J. Tian, S. Xie, Y. Pei, M. Qiao and B. Zong, *Appl. Catal., B*, 2017, **217**, 331–341.
- 43 K. Narasimha Rao, A. Sridhar, A. F. Lee, S. J. Tavener, N. A. Young and K. Wilson, *Green Chem.*, 2006, **8**, 790–797.
- 44 A. Guntida, K. Suriye, J. Panpranot and P. Praserthdam, *Catal. Today*, 2020, **358**, 354–369.
- 45 D. G. Barton, M. Shtein, R. D. Wilson, S. L. Soled and E. Iglesia, *J. Phys. Chem. B*, 1999, **103**, 630–640.
- 46 S. E. Hobsley, D. V. Nowell and D. T. Stewart, *Spectrochim. Acta*, 1974, **30A**, 535–541.
- 47 T. Aihara, H. Miura and T. Shishido, *Catal. Today*, 2020, **352**, 73–79.
- 48 S. Feng, A. Nagao, T. Aihara, H. Miura and T. Shishido, *Catal. Today*, 2018, **303**, 207–212.
- 49 K. Tomishige, Y. Nakagawa and M. Tamura, *Green Chem.*, 2017, **19**, 2876–2924.